

# Full-waveform inversion for salt: A coming of age

Ping Wang<sup>1</sup>, Zhigang Zhang<sup>1</sup>, Jiawei Mei<sup>1</sup>, Feng Lin<sup>1</sup>, and Rongxin Huang<sup>1</sup>

<https://doi.org/10.1190/tle38030204.1>

## Abstract

Full-waveform inversion (FWI), proposed by Lailly and Tarantola in the 1980s, is considered to be the most promising data-driven tool for automatically building velocity models. Many successful examples have been reported using FWI to update shallow sediments, gas pockets, and mud volcanoes. However, successful applications of FWI to update salt structures had almost only been seen on synthetic data until recent progress at the Atlantis Field in the Gulf of Mexico. We revisited some aspects of FWI algorithms to minimize cycle-skipping and amplitude discrepancy issues and derived an FWI algorithm that is able to build complex salt velocity models. We applied this algorithm to a variety of data sets, including wide-azimuth and full-azimuth (FAZ) streamer data as well as ocean-bottom-node data, with different geologic settings in order to demonstrate the effectiveness of the method for salt velocity updates and to examine some fundamentals of the salt problem. We observed that, in multiple cases, salt velocity models from this FWI algorithm produced subsalt images of superior quality. We demonstrate with one FAZ streamer data example in Keathley Canyon that we do not necessarily need very high frequency in FWI for subsalt imaging purposes. Based on this observation, we envision that sparse node for velocity acquisition may provide appropriate data to handle large and complex salt bodies with FWI. We believe the combination of advanced FWI algorithms and appropriate data acquisition will bring a step change to subsalt imaging.

## Introduction

Subsalt images can be very sensitive to the accuracy of the salt model because salt misinterpretation can easily lead to large timing errors and significant deviation of wave paths. Therefore, among other factors, one key to successful subsalt imaging is building accurate salt velocity models. For decades, the standard practice for salt model building has been to use tomography, sometimes combined with shallow diving-wave full-waveform inversion (FWI), to first build the best possible sediment velocity model. Then, a sediment-flood migration is used for top-of-salt (TOS) interpretation followed by a salt-flood migration for base-of-salt (BOS) interpretation. In the next step, a number of salt scenario tests are usually required to resolve the salt geometry, especially for complex areas. This procedure is not only labor intensive and time consuming, but it is also prone to human misinterpretation.

FWI is considered the most promising data-driven tool to automatically build velocity models by iteratively minimizing the difference between recorded data and modeled synthetic data (Lailly, 1983; Tarantola, 1984; Pratt, 1999; Sirgue and Pratt, 2004). Using the BP 2004 salt model (Billette and Brandsberg-Dahl, 2005), Brenders and Pratt (2007) demonstrate that it is

possible to use FWI to build a salt velocity model from a smooth initial model. However, they use frequencies as low as 0.5 Hz for this, which is much lower than what normally exists in our field data. Since then, many papers have reported the ability to update salt velocity with FWI using synthetic data (Esser et al., 2015; Datta et al., 2016; Guasch et al., 2016; Kadu et al., 2016). However, these approaches have yet to demonstrate consistent success in real-data applications.

A breakthrough success of FWI salt velocity updating came from Shen et al. (2017) and Michell et al. (2017) in which FWI corrected some misinterpretation of salt structures, resulting in greatly improved subsalt images at the Atlantis Field in the Gulf of Mexico (GOM). These studies stress the importance of the low frequencies (usable down to 1.6 Hz), full azimuths, and long offsets of ocean-bottom-node (OBN) data as well as an innovative FWI algorithm/workflow. Encouraged by the success at Atlantis, Zhang et al. (2018) revisit some aspects of FWI algorithms to minimize cycle-skipping and amplitude discrepancy issues (Luo and Schuster, 1991; Ma and Hale, 2013) that are common in the presence of salt and salt misinterpretation. These investigations led to a new FWI approach called time-lag FWI (TLFWI) (Zhang et al., 2018). It uses a time-lag cost function (Luo and Schuster, 1991; Chavent et al., 1994) to reduce amplitude errors in the standard data-mismatch cost function (Tarantola, 1984). In addition, it uses frequency-dependent time windows for time-lag measurements and the crosscorrelation coefficient between recorded data and synthetic data as a weight function in the gradient computation to promote traveltimes measurements of higher quality. This allows TLFWI to start from a lower frequency than conventional FWI, which typically uses the squares of data difference as the cost function; this is important for mitigating cycle skipping. TLFWI is mostly driven by diving-wave energy, though reflection data were also found to be useful but only if the diving-wave energy is adequate for FWI to provide a good enough low-wavenumber background velocity model. In the next sections, we apply TLFWI for salt velocity updates on different types of input data sets, including wide-azimuth (WAZ) and full-azimuth (FAZ) streamer data and OBN data, with different levels of salt complexity. This leads to an examination of some fundamentals of the salt problem and a proposal for the optimal acquisition type for handling large and complex salt bodies with FWI.

## Salt velocity updating with FWI

The first study area is located in Keathley Canyon in the central GOM, which is to the interior of the Sigsbee Escarpment. It features complex salt structures (blue box in Figure 1a). The data were acquired using multiple vessels in a staggered configuration (Figure 1b) that provided FAZ coverage up to 10 km and ultra-long offsets up to 18 km (Figure 1c). The towed streamers

<sup>1</sup>CGG, Houston, Texas, USA. E-mail: ping.wang@cgg.com; zhigang.zhang@cgg.com; jiawei.mei@cgg.com; feng.lin@cgg.com; rongxin.huang@cgg.com.

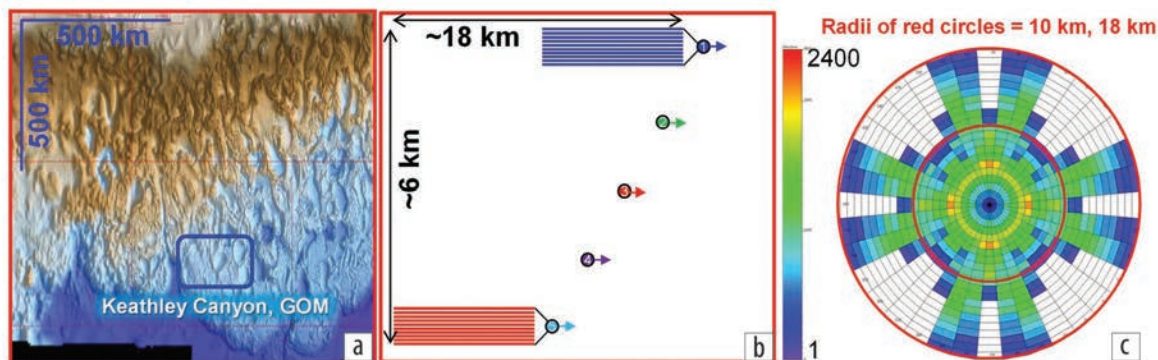


**Figure 1.** (a) Bathymetry in Keathley Canyon, GOM. (b) Staggered streamer acquisition geometry. (c) Rose diagram considering reciprocity. The inner circle marks 10 km offset, and the outer circle represents 18 km offset. The color bar represents the fold.

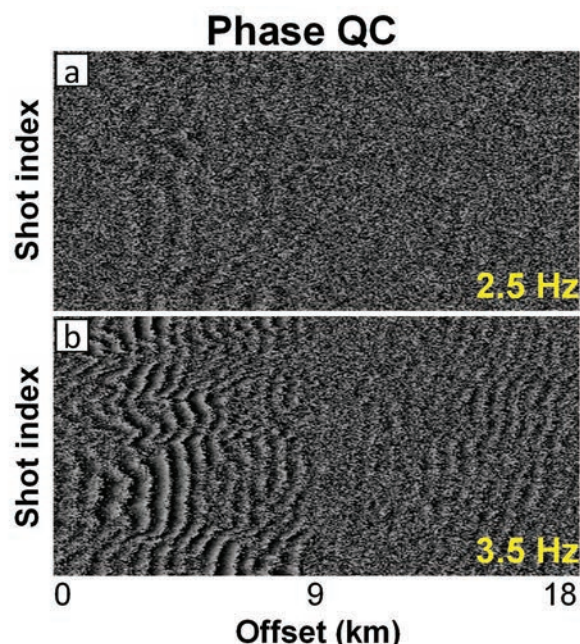


**Figure 2.** Phase quality control (QC) of the center cable for shots from one sail line at (a) 2.5 Hz and (b) 3.5 Hz. The S/N at 2.5 Hz is very low and we needed to start our prior FWI approaches, TLFWI (Zhang et al., 2018), from 3.5 Hz.

had variable depths ranging between 10 and 50 m (Mandrourx et al., 2013), providing observable low-frequency signals down to 2.5 Hz (Figure 2a). Although not as good as the Atlantis OBN data in terms of azimuth, offset, and low frequency, this is still one of the best streamer data sets to tackle the complex salt problem with FWI.

The legacy velocity model (Figure 3a) was obtained after several iterations of ray-based reflection tomography and conventional diving-wave FWI only for the shallow-sediment velocity updates followed by typical manual salt interpretation and subsalt velocity updates. It is not obvious to understand how the complex salt geometry in the middle portion was obtained with manual salt interpretation, given the poor legacy reverse time migration (RTM) image in Figure 3b that does not provide clear hints of salt boundaries. Nevertheless, the model in Figure 3a was the best salt model we were able to obtain after numerous salt scenario tests. However, the poor subsalt image below the complexity tells us that “the best salt model” we obtained is still far from good.

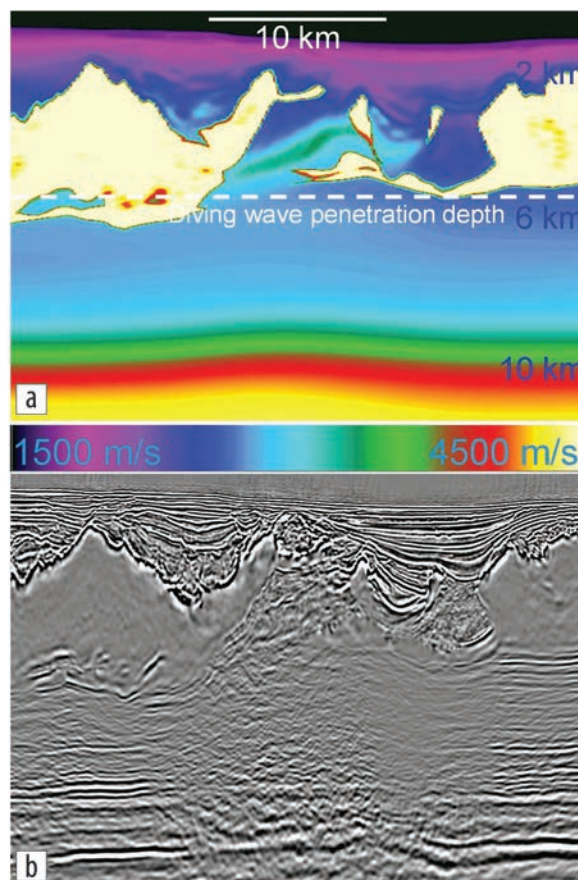


**Figure 3.** Inline section in Keathley Canyon in the deepwater GOM. (a) Legacy velocity model and (b) RTM stack image. The color bar in the center is for the velocity model in (a). The same color bar is used for the velocity models in all figures.

The initial velocity model to our TLFWI (later referred to as FWI where there is no ambiguity) workflow was derived from the legacy model after applying a smoother with a radius of about 500 m to remove the potentially erroneous sharp salt boundaries (Figure 4a). (The same procedure was adopted for all the later FWI examples.) We ran FWI with frequency continuation from 2.5 to 8 Hz. We note that in our prior FWI approaches, we needed to start from 3.5 Hz (Figure 2b) because the signal-to-noise ratio (S/N) at 2.5 Hz (Figure 2a) is extremely low, and thus starting from 2.5 Hz did more harm than good. We observed that FWI

introduced a mixture of salt and sediment in the middle portion (white oval in Figure 4b), which is very different from the manual salt interpretation (Figure 3a). The image created with this new FWI model is the best image we have seen in this area (Figure 4d). However, we still observed a couple of obvious problems: (1) the salt boundaries are smooth, and (2) there are still imaging gaps and strong migration artifacts right below the middle complexity (white ovals in Figure 4d). Despite the imperfections, we were excited to see FWI finally working to update the salt velocity model and improve the subsalt image. More importantly, it enabled us to investigate some fundamentals of the salt problem that may offer hints for further improvements in the subsalt image in this area and other areas in the GOM.

### Do we need high-frequency FWI?

In the example shown earlier, despite the fact that FWI does not give a velocity model with sharp salt boundaries, the uplift of the RTM image migrated using the velocity model directly from FWI is substantial. As we mentioned, subsalt images can be very sensitive to the accuracy of the salt velocity model. Does this mean there is still room to further improve the subsalt imaging if we can obtain a salt velocity model with sharper boundaries using higher frequency FWI? Theoretically, to resolve abrupt velocity jumps at the salt boundary with FWI requires infinitely high frequency or up to the Nyquist frequency imposed by temporal

and spatial sampling of the input data and wave-propagation engine. However, the highest frequency we can use is often limited by compute cost and hardware (memory, disk space, bandwidth, etc.). Therefore, it is important to find the maximum frequency for FWI, which results in the “sweet spot” of giving the best uplift in the migration image without being so high as to be impractical on today’s current computational hardware. To establish the possible benefit of high-frequency FWI for subsalt imaging, we need the salt body to be well sampled by diving waves and the initial velocity error to not be too large, allowing the FWI inversion to converge toward the correct solution from low to high frequencies. Based on such criteria, with the Keathley Canyon data example of the previous section, we identified a test area where the salt body is shallow (3 to 4 km) and therefore well penetrated by the diving waves in this data set, and the salt geometry is relatively simple so that the velocity error may not be too large for the initial model for FWI.

Figure 5a shows the legacy velocity model with the unsmoothed salt body, and Figure 5b shows the corresponding RTM stack image using the legacy velocity model in Figure 5a. As we expected, the salt boundary became sharper and the subsalt image improved as the FWI frequency increased from 2.5 to 8 Hz, culminating in Figures 5c and 5d. Figure 5c shows the velocity model from 8 Hz FWI that gave rise to the image in Figure 5d. There are several features in this velocity model to note: (1) the salt body is

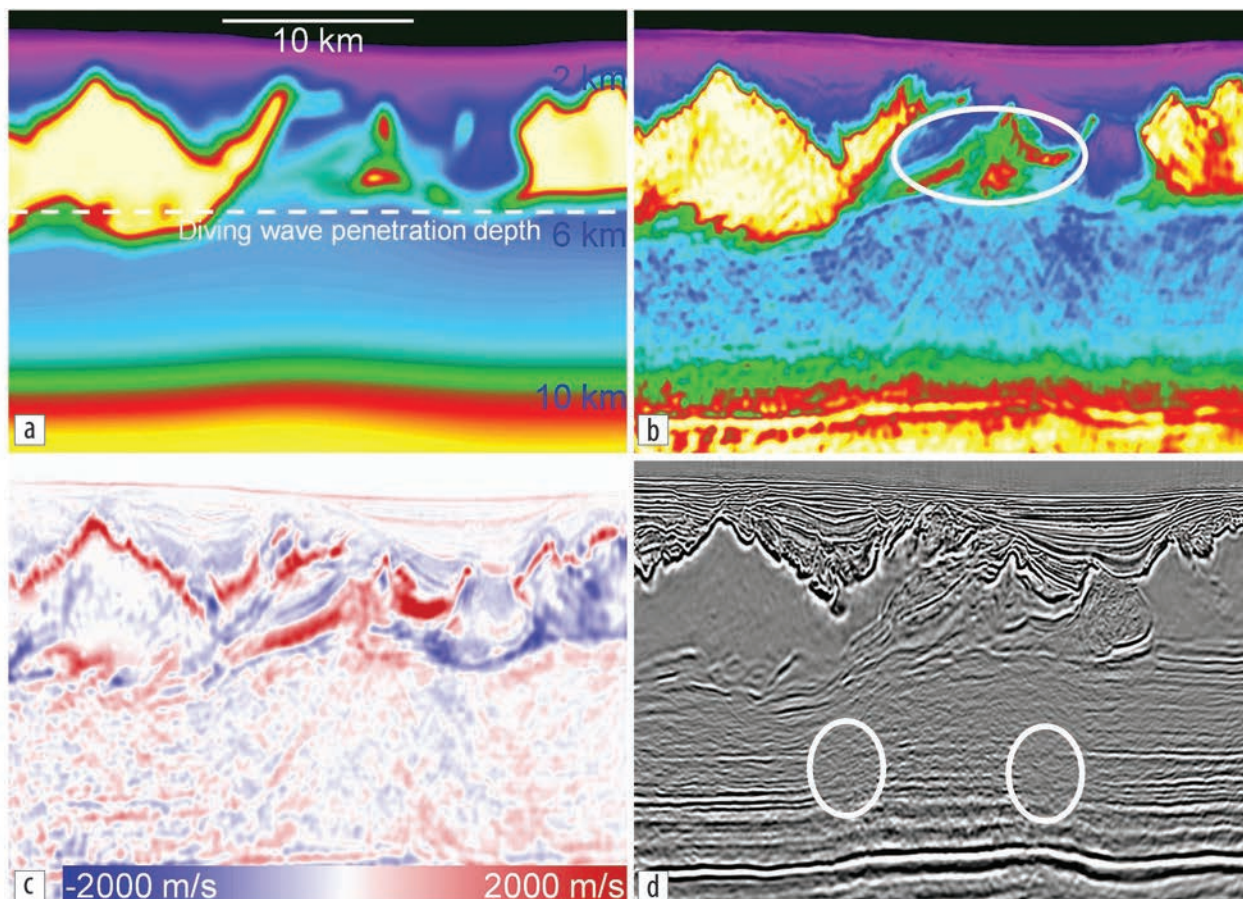


**Figure 4.** (a) Initial model for FWI, (b) 8 Hz FWI velocity model, (c) 8 Hz FWI velocity perturbation, and (d) RTM stack image produced using the FWI-updated velocity model in (b).

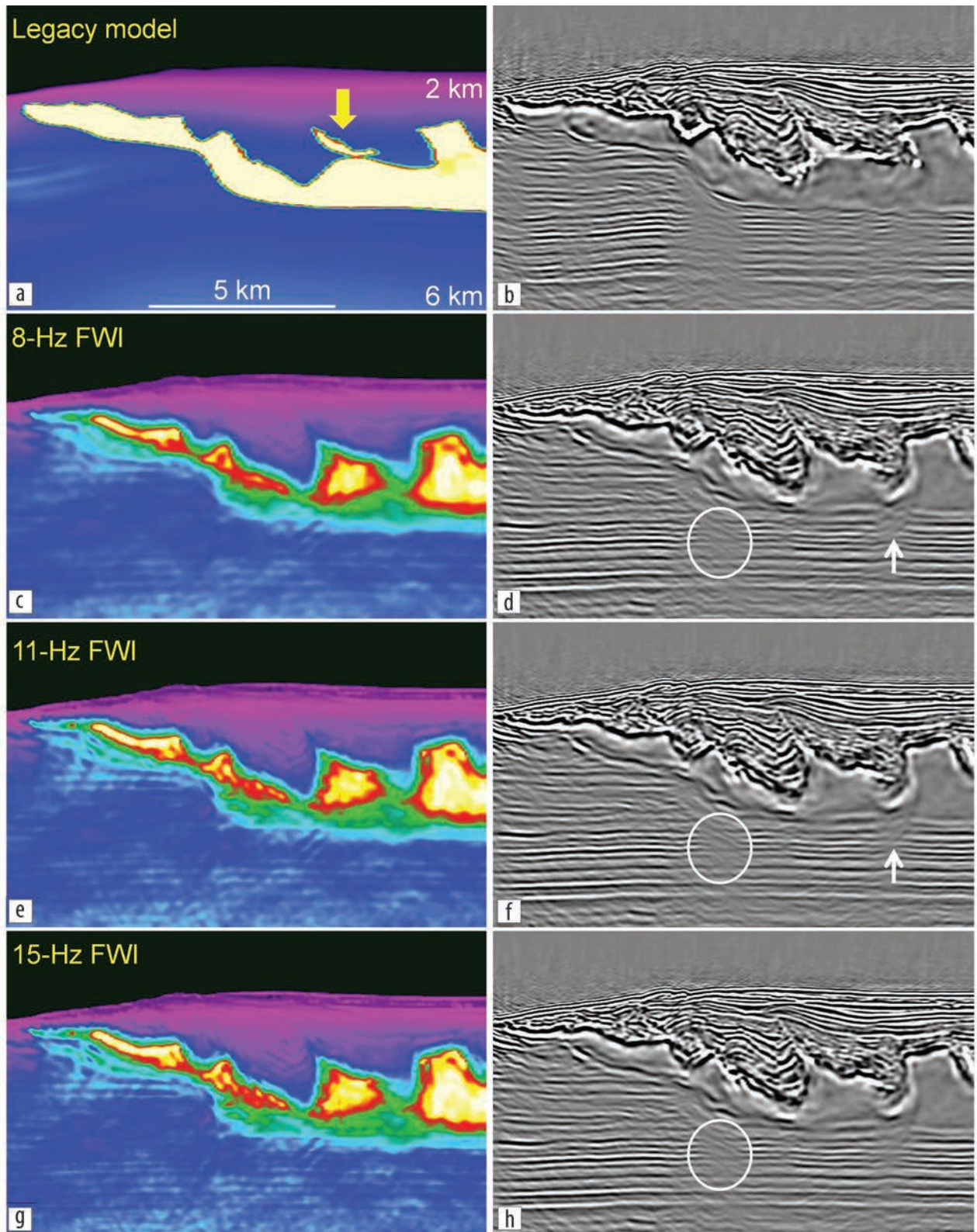


Figure 5. Velocity model and RTM stack image for the (a)/(b) legacy model without any smoothing, the (c)/(d) 8 Hz, (e)/(f) 11 Hz, and (g)/(h) 15 Hz FWI velocity models.

smaller than the one in the legacy velocity model, especially on the far left; (2) the salt finger in the center of the legacy model is much less visible in the FWI model than in Figure 5a (yellow arrow); (3) the salt boundary is smooth; and (4) there is obvious high-wavenumber migration leakage (horizontal striping due to horizontal reflectors) in the subsalt velocity model. Compared to the legacy image in Figure 5b, the RTM image after 8 Hz FWI (Figure 5d) has better focusing with improved event continuity and reduced migration artifacts. The improvement in the subsalt image is most noticeable on the far left where the salt geometry has been altered the most by FWI. We can still observe a major imaging gap (white oval in Figure 5d) just below the places where the TOS appears to be very complex and may still contain relatively large velocity errors that were not fully corrected by 8 Hz FWI.

To see how higher frequency FWI will impact the velocity model and migrated image, we continued running FWI up to 15 Hz. Figure 5e shows the velocity model after 11 Hz FWI. Compared to the 8 Hz FWI velocity model in Figure 5c, the 11 Hz FWI velocity model has a similar low-wavenumber background with two differences: (1) the salt boundary is sharper, as expected, and (2) the migration term in the subsalt velocity model has even higher wavenumbers. While some fine-scale imaging uplift can be observed right beneath a TOS complexity (white arrow in Figure 5f), as well as some tiny-scale focusing differences mostly due to the high-wavenumber migration leakage in the

FWI velocity model, the overall image difference between 8 Hz (Figure 5d) and 11 Hz FWI (Figure 5f) is very small. This indicates that, for this example, the migration image quality is driven mostly by the low-wavenumber background velocity model. The high-wavenumber migration term and the sharpness of the salt boundary in the FWI velocity model have little impact on the kinematics during migration after 8 Hz. Not surprisingly, the image difference between 15 Hz (Figure 5h) and 11 Hz FWI (Figure 5f) is negligible even though the high-wavenumber difference between their velocity models (Figures 5e and 5g) is not small, similar to the comparison between 11 and 8 Hz FWI. This means that for this data example, most of the imaging benefit comes from FWI below 8 Hz; the additional imaging benefit from going beyond 11 Hz FWI is negligible.

### What are the right data for salt-related FWI?

With the previous examples from Keathley Canyon, we demonstrated that FWI is able to partly resolve salt misinterpretation and thus improve the subsalt image when the salt body is shallow (< 6 km) and therefore reasonably well sampled by diving-wave energy from a staggered variable-depth streamer data set (full azimuth up to 10 km, maximum offset up to 18 km, and low frequency down to 2.5 Hz). In this section, we first illustrate the performance of FWI with different data sets on different salt geometries and then propose possible data acquisition

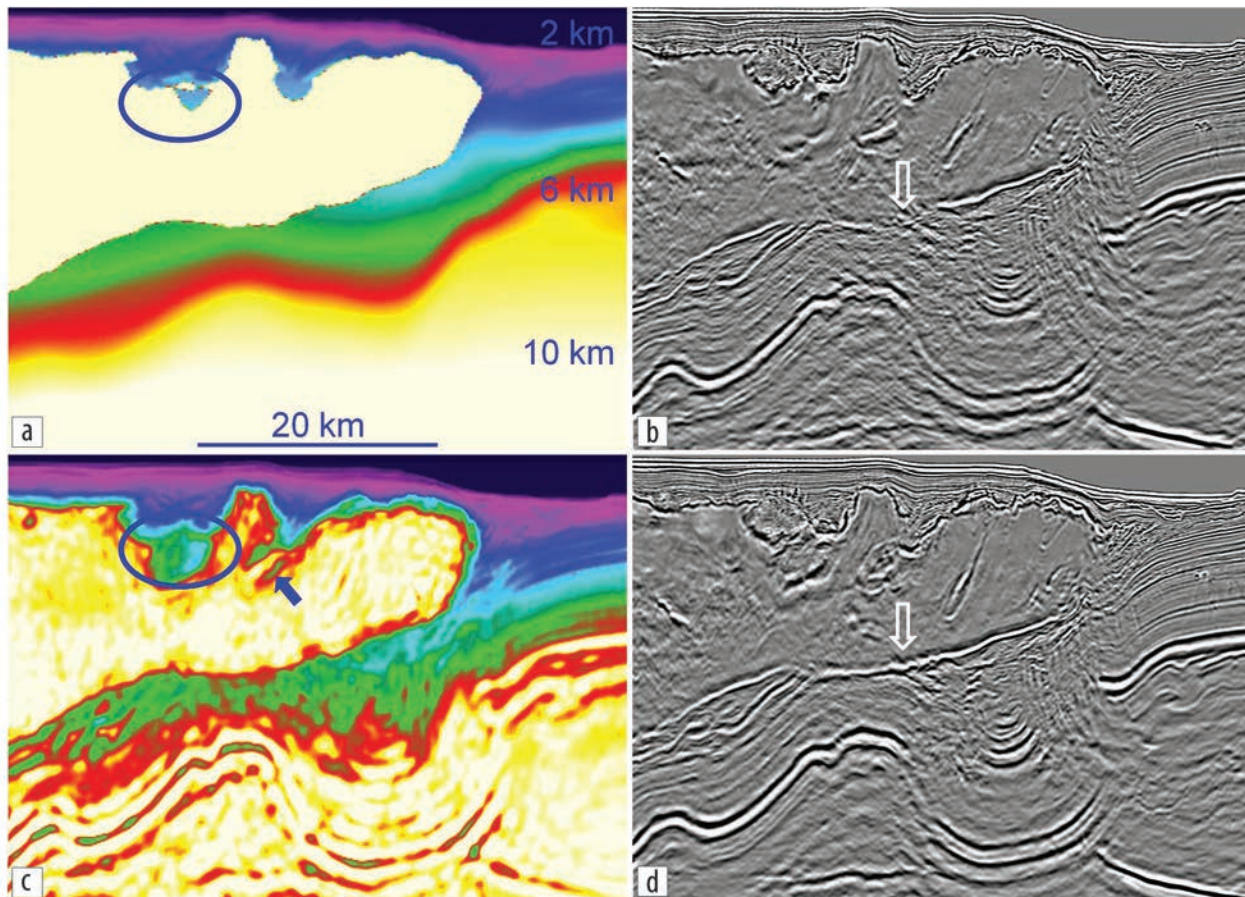


**Figure 6.** FWI using CWAZ data in an area with shallow rugose TOS. Inline section before the FWI update: (a) legacy velocity model without smoothing and (b) RTM stack image produced using the legacy model. Inline section after the FWI update: (c) FWI-updated velocity model and (d) RTM stack image produced using the FWI-updated velocity model.

configurations that may be conducive to resolving the salt velocity model with FWI in different geologic settings.

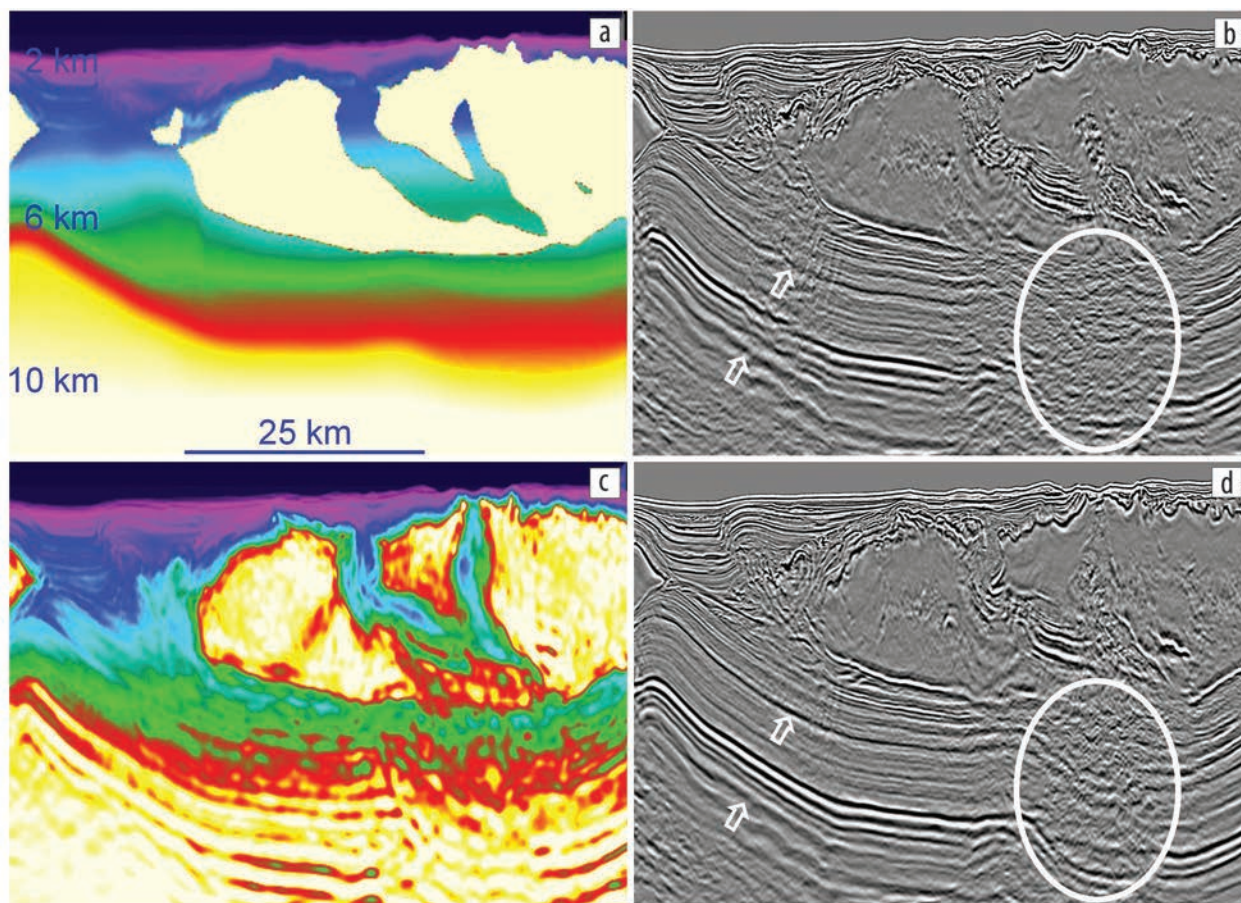
**WAZ data example.** The input data were acquired using the so-called complementary wide-azimuth (CWAZ) geometry. The lowest usable frequency is down to 2.5 Hz because variable-depth streamers were used. However, its offset coverage is much narrower than the staggered streamer data used in previous examples, with an inline offset of only 15 km and crossline offset of less than 6 km. The study area is located in Alaminos Canyon in the deepwater GOM. This area is famous for a rugose TOS that poses tremendous difficulties for manual salt interpretation. In addition, the salt body in this area is fairly large with a depth ranging from 6 to 8 km, which makes diving waves from CWAZ data insufficient to sample the whole salt body.

Figure 6b shows the RTM image using the legacy velocity model. We observed that the image of the TOS is very complex and not clear. The salt geometry in the velocity model in Figure 6a was the best we could obtain after many rounds of a conventional velocity model building (VMB) flow that included ray-based tomography, shallow-sediment FWI, and salt scenarios. However, we observed an image gap at the BOS, as indicated by the arrow in Figure 6b. This indicates problems with the salt model above. Figure 6c shows the 7 Hz FWI velocity model. The most noticeable change is that FWI extended the sediment in the blue oval deeper into the salt body. It also added a small overhang and a small

sediment inclusion into the salt body, as indicated by the blue arrow. As a result, both the BOS image and the subsalt image are improved (Figure 6d) with the FWI velocity model. This greatly exceeded our expectations. We believe the improvement occurred because most of the velocity error is around the TOS that is shallow enough to be well illuminated by the diving waves from CWAZ data. Therefore, FWI could reasonably correct the velocity error and thus improve the image, although we expect velocity errors may still exist at greater depths around the BOS, which is well beyond the reach of diving-wave penetration from CWAZ data.

It was not difficult for us to find another location in the same area where FWI is set to fail with CWAZ data. Compared to the legacy RTM image in Figure 7b, we observed decent imaging uplift on the left because most of the velocity error was concentrated at shallow depths and thus could be reasonably corrected by FWI (Figure 7d). Moving to the right, we observe a very complex sediment inclusion deep within the salt body, which likely contains large velocity errors but is beyond the diving-wave coverage of CWAZ data. It is not surprising that FWI failed to improve the subsalt image beneath this deep and complex salt body (white oval in Figure 7d). OBN data with full azimuth, longer offsets, and better low frequency are desired in this case for FWI to update the deep and complex salt velocity model.

**OBN data example.** This study area is also in the deepwater GOM. From the legacy velocity model (Figure 8a) and OBN



**Figure 7.** FWI using CWAZ data in an area with complex sediment inclusions in a large and deep salt body. Inline section before the FWI update: (a) legacy velocity model without smoothing and (b) RTM stack image produced using the legacy model. Inline section after the FWI update: (c) FWI-updated velocity model and (d) RTM stack image produced using the FWI-updated velocity model in (c).

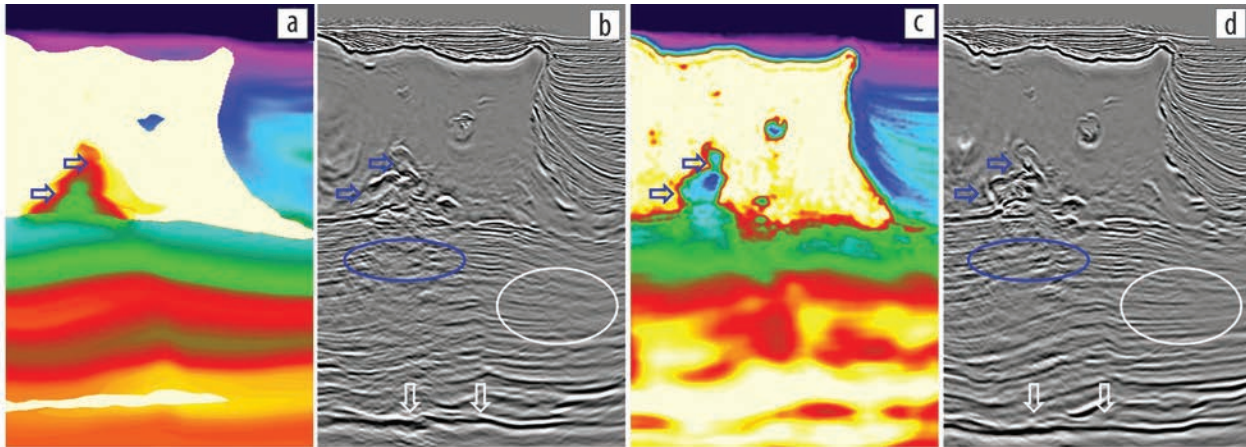


**Figure 8.** FWI using OBN data in an area with a complex sediment-salt interface close to the deep BOS. Inline section before the FWI update: (a) legacy velocity model without smoothing and (b) OBN RTM stack image produced using the legacy model. Inline section after the FWI update: (c) updated velocity model from FWI using OBN data and (d) OBN RTM stack image produced using the FWI-updated velocity model in (c).

RTM stack image (Figure 8b), we observed that the TOS is simple and well resolved with our conventional VMB flow. However, there is a piece of ambiguous sediment around the BOS in the center. The legacy model was obtained after multiple rounds of reprocessing that involved numerous scenario tests combined with ray-based tomography and shallow legacy FWI (which was ineffective for salt). The poor image below the complexity told us that we did not get the details of the sediment-salt interface correct around the BOS (blue arrows in Figure 8a).

Figure 8c shows the 8 Hz TLFWI velocity model using FAZ, long-offset, and good low-frequency OBN data. There are a few noticeable changes brought about by FWI. First, the salt-sediment interface (blue arrows) is now better defined than in the legacy velocity model (Figure 8a). Second, FWI reduced the size of the salt weld at the bottom right of the salt body. Third, FWI added some small sediment inclusions in the salt body and fine tuned the salt boundary at various places. The OBN RTM image created using the FWI velocity model is shown in Figure 8d. Several major imaging uplifts can be observed. First, the image of the salt-sediment interface around the BOS in the center is better defined and better correlates with the velocity model in Figure 8c (blue arrows). Second, the image just below the sediment body in the center is better focused with improved event continuity (blue oval). Third, the subsalt events on the far right become more focused and extend farther to the right after the size reduction of the salt weld by FWI (white oval). Fourth, the strong basement event at the very bottom is better focused and connected through the whole inline section (white arrows). Last, the overall subsalt image is cleaner and simpler with reduced migration swings and improved focusing.

**Sparse node for velocity data.** Among all the existing data types, OBN data are no doubt the best for FWI purposes, given

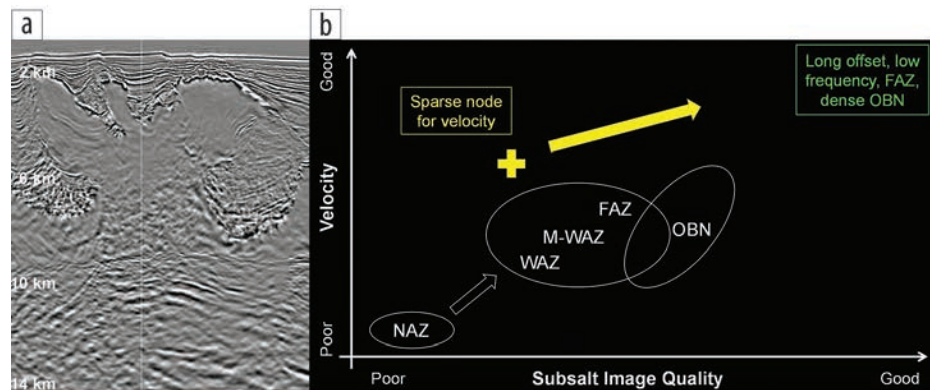


**Figure 9.** (a) An example with a large and complex salt body. (b) Image and velocity quality for different acquisition geometries. The green box stands for high-end OBN, and the yellow box represents sparse NFV. The plus sign indicates a combination of sparse NFV (velocity inversion with FWI) and existing data (migration) for subsalt imaging.

the full azimuth, long offsets, and good low-frequency S/N. However, there are areas in the GOM where the salt body is so large and so complex in geometry (Figure 9a) that it is beyond resolvability for typical OBN data. For example, with a depth of approximately 10 km, the salt body here would likely require offsets of up to approximately 30 km or longer to be fully illuminated by diving waves. In addition to its extraordinary size, the salt geometry is very complex with overhangs, sediment inclusions, and sutures. In this case, our conventional VMB flow may completely fail to provide a reasonably good velocity model as the initial model for FWI. Therefore, ultra-low frequency may be required to deal with the possible severe cycle-skipping issues. In addition, FAZ and dense node sampling would be helpful for tackling the complex and fine details of the salt model and providing high fold and good illumination for subsalt imaging. The ultimate solution is therefore to acquire high-end OBN data that are superior not only for FWI velocity model updating but also for subsalt imaging with even longer offsets, lower frequency, and denser node sampling than existing OBN data sets (green box in Figure 9).

Of course, obtaining high-end OBN data for large-scale exploration purposes can be financially challenging. One

alternative is to acquire sparse node for velocity (NFV) data for velocity purposes only (yellow box in Figure 9) (Dellinger et al., 2017). As we have shown, an 8 Hz FWI velocity model can significantly improve the subsalt image even if it does not recover the sharp salt boundary. Therefore, sparser shot and node sampling can be used to fit the purpose of updating the velocity model with FWI to improve the subsalt imaging. With sparser shot and node sampling, it becomes feasible to acquire ultra-long offsets and expand the survey coverage, which not only makes it easier for FWI to deal with large and complex salt bodies but also allows OBN data to be used for large-scale exploration purposes.

If FWI works on sparse NFV data as expected to provide better salt velocity models, we can migrate existing streamer or node data to obtain improved subsalt images (Figure 9b). This would be an economic yet adequate way to improve our subsalt imaging.

## Discussion

FWI was first proposed by Lailly and Tarantola in the 1980s. It took about 30 years to make it work for salt velocity updates on field data (Shen et al., 2017, 2018a; Zhang et al., 2018). In various cases, we have seen its ability to produce subsalt images of unprecedented quality. However, we are still at the low end of the learning curve for salt velocity updating with FWI. A year ago, we attributed the failure of our legacy FWI for salt velocity updates to insufficient data. In 2018, we realized that our data were better than our legacy FWI algorithms. Now, with an improved TLFWI algorithm that works reasonably for salt velocity updates, we are confident we can improve subsalt images by further improving our FWI algorithm/workflow and acquiring more appropriate data.

We demonstrated with data examples in Keathley Canyon that high-frequency FWI is not always required for subsalt imaging. However, we are not suggesting that high-frequency FWI has no value. First, running FWI to a higher frequency can be important for applications where accurate salt-sediment boundary information is required (e.g., drilling markers). Second, it is possible to see imaging benefits from higher frequency FWI when errors from other factors, such as insufficient illumination and inaccurate physics (e.g., density, absorption, anisotropy, and elasticity), are small enough. Third, there has been some discussion about the possibility of directly interpreting the high-frequency FWI velocity model (Lu, 2016; Shen et al., 2018b), even though the high-frequency component of the velocity model may not have much impact on the migration kinematics. However, one needs to be aware that the high-frequency FWI velocity model can be contaminated by inadequate physics (e.g., density, absorption, anisotropy, and elasticity may not be modeled or allowed to change during FWI) in the inversion algorithm, and therefore its interpretation must be performed with care.

Various studies have suggested using reflection energy for deep velocity updates with ray-based tomography (Yang et al., 2015) and reflection FWI (Mora, 1989; Xu et al., 2012; Tang et al., 2013; Irabor and Warner, 2016). However, it has been challenging to use such approaches to obtain reliable salt velocity updates because of the limited angle coverage of the reflection

data from subsalt reflectors and the requirement of good focusing of subsalt reflection events for curvature picking in ray-based tomography (Yang et al., 2015) or generation of “rabbit ears” in reflection FWI (Gomes and Chazalnoel, 2017; Jonke et al., 2017; Wang et al., 2018). Therefore, ultra-long-offset data such as high-end OBN or sparse NFV are desired for applying diving-wave FWI to large complex salt bodies. However, the S/N of the low-frequency data drops quickly with increasing offset. In addition, the ability to handle noise with stacking power in FWI is reduced with sparse shot and node sampling. To overcome such problems, using a powerful low-frequency source (Dellinger et al., 2016) to improve the low-frequency S/N may be very important for sparse NFV surveys. Additional research on pushing the frequency of the source even lower may be another key to improving our data for FWI salt velocity updates. Furthermore, how sparsely we may space the nodes and shots is difficult to assess in general because optimal node/shot sampling is likely dependent on the geologic setting, and it is not an easy task to transfer modeling results into actual operations owing to the large gap that often exists between modeled and recorded data (Dellinger et al., 2017).

During the course of preparing this paper, we learned that the industry is planning to acquire more than 10 OBN data sets in the GOM in the coming year, including a few sparse NFV data sets. As in the last seismic acquisition and imaging technology revolution that started around 2005 when the industry transitioned from NAZ to WAZ and then FAZ acquisition (Michell et al., 2006; Threadgold et al., 2006; Moldoveanu and Kapoor, 2009; Mandroux et al., 2013), we expect there will be much excitement and many opportunities during this new revolution fueled by OBN acquisition and FWI. It is worth noting that in all the examples shown here, we performed FWI to update the velocity model only as it is still challenging to see the benefit from updating other parameters such as anisotropy, density, and absorption, although we did include these parameters to generate synthetic data to compare with recorded data within FWI. With more appropriate data, we should be able to further improve our FWI algorithms for salt velocity updates and may be able to better constrain other parameters and see the additional benefit from joint or alternating multiparameter FWI.

## Conclusions

We demonstrated that with an improved algorithm, FWI is able to build complex salt velocity models with different types of input data including WAZ and FAZ streamer data as well as OBN data in different areas. The resulting subsalt images are the best images we have seen in those areas, although there is room for further improvement. We also demonstrated with a data set in Keathley Canyon that FWI with a frequency higher than 11 Hz is not always required for subsalt imaging purposes. We then discussed the need for high-end OBN data or sparse NFV data to handle large and complex salt bodies. We expect to further improve our FWI algorithm with more appropriate data and as we gain more experience in salt velocity updating with FWI. The combination of more suitable data and further improved FWI algorithms should enable us to make a leap forward in subsalt imaging. **TLE**

## Acknowledgments

We thank Hess and CGG Multi-Client and New Ventures for permission to show the data examples. We are grateful to numerous CGG colleagues for successfully applying the TLFWI workflow to different data sets.

## Data and materials availability

Data associated with this research are confidential and cannot be released.

Corresponding author: ping.wang@cgg.com

## References

- Billette, F. J., and S. Brandsberg-Dahl, 2005, The 2004 BP velocity benchmark: 67<sup>th</sup> Conference and Exhibition, EAGE, Extended Abstracts, B035.
- Brenders, A. J., and R. G. Pratt, 2007, Waveform tomography of marine seismic data: What can limited offset offer?: 77<sup>th</sup> Annual International Meeting, SEG, Expanded Abstracts, 3024–3028, <https://doi.org/10.1190/1.2793099>.
- Chavent, G., F. Clément, and S. Gómez, 1994, Automatic determination of velocities via migration-based traveltime waveform inversion: A synthetic data example: 64<sup>th</sup> Annual International Meeting, SEG, Expanded Abstracts, 1179–1182, <https://doi.org/10.1190/1.1822731>.
- Datta, D., M. Sen, F. Liu, and S. Morton, 2016, Salt model building by shape-based parameterization and global FWI: 86<sup>th</sup> Annual International Meeting, SEG, Expanded Abstracts, 1069–1073, <https://doi.org/10.1190/segam2016-13867592.1>.
- Dellinger, J., A. Brenders, J. R. Sandschaper, C. Regone, J. Etgen, I. Ahmed, and K. J. Lee, 2017, The Garden Banks model experience: The Leading Edge, **36**, no. 2, 151–158, <https://doi.org/10.1190/tle36020151.1>.
- Dellinger, J., A. Ross, D. Meaux, A. Brenders, G. Gesoff, J. Etgen, J. Naranjo, G. Openshaw, and M. Harper, 2016, Wolfspär®, an “FWI-friendly” ultralow-frequency marine seismic source: 86<sup>th</sup> Annual International Meeting, SEG, Expanded Abstracts, 4891–4895, <https://doi.org/10.1190/segam2016-13762702.1>.
- Esser, E., L. Guasch, T. van Leeuwen, A. Aravkin, and F. J. Herrmann, 2015, Automatic salt delineation — Wavefield reconstruction inversion with convex constraints: 85<sup>th</sup> Annual International Meeting, SEG, Expanded Abstracts, 1337–1343, <https://doi.org/10.1190/segam2015-5877995.1>.
- Gomes, A., and N. Chazalnoel, 2017, Extending the reach of full-waveform inversion with reflection data: Potential and challenges: 87<sup>th</sup> Annual International Meeting, SEG, Expanded Abstracts, 1454–1459, <https://doi.org/10.1190/segam2017-17731403.1>.
- Guasch, L., M. Warner, and F. J. Herrmann, 2016, Constrained waveform inversion — Automatic salt flooding with inclusions: 78<sup>th</sup> Conference and Exhibition, EAGE, Extended Abstracts, <https://doi.org/10.3997/2214-4609.201601547>.
- Irabor, K., and M. Warner, 2016, Reflection FWI: 86<sup>th</sup> Annual International Meeting, SEG, Expanded Abstracts, 1136–1140, <https://doi.org/10.1190/segam2016-13944219.1>.
- Jonke, K., Z. Fu, B. Wray, and H. Shen, 2017, Improving minibasin and subsalt imaging with reflection full-waveform inversion: 87<sup>th</sup> Annual International Meeting, SEG, Expanded Abstracts, 1492–1496, <https://doi.org/10.1190/segam2017-17661070.1>.
- Kadu, A., T. van Leeuwen, and W. Mulder, 2016, A parametric level-set approach for seismic full-waveform inversion: 86<sup>th</sup> Annual International Meeting, SEG, Expanded Abstracts, 1146–1150, <https://doi.org/10.1190/segam2016-13870276.1>.
- Lailly, P., 1983, The seismic inverse problem as a sequence of before stack migrations: Conference on inverse scattering: Theory and application, Society for Industrial and Applied Mathematics, 206–220.
- Lu, R., 2016, Revealing overburden and reservoir complexity with high-resolution FWI: 86<sup>th</sup> Annual International Meeting, SEG, Expanded Abstracts, 1242–1246, <https://doi.org/10.1190/segam2016-13872562.1>.
- Luo, Y., and G. T. Schuster, 1991, Wave-equation traveltime inversion: Geophysics, **56**, no. 5, 645–653, <https://doi.org/10.1190/1.1443081>.
- Ma, Y., and D. Hale, 2013, Wave-equation reflection traveltime inversion with dynamic warping and hybrid waveform inversion: 83<sup>rd</sup> Annual International Meeting, SEG, Expanded Abstracts, 871–876, <https://doi.org/10.1190/segam2013-0087.1>.
- Mandroux, F., B. Ong, C. Ting, S. Mothi, T. Huang, and Y. Li, 2013, Broadband, long-offset, full-azimuth, staggered marine acquisition in the Gulf of Mexico: First Break, **31**, no. 6, 125–132.
- Michell, S., E. Shoshitaishvili, D. Chergotis, J. Sharp, and J. Etgen, 2006, Wide azimuth streamer imaging of Mad Dog: Have we solved the subsalt imaging problem?: 76<sup>th</sup> Annual International Meeting, SEG, Expanded Abstracts, 2905–2909, <https://doi.org/10.1190/1.2370130>.
- Michell, S., X. Shen, A. Brenders, J. Dellinger, I. Ahmed, and K. Fu, 2017, Automatic velocity model building with complex salt: Can computers finally do an interpreter’s job?: 87<sup>th</sup> Annual International Meeting, SEG, Expanded Abstracts, 5250–5254, <https://doi.org/10.1190/segam2017-17778443.1>.
- Moldoveanu, N., and J. Kapoor, 2009, What is the next step after WAZ for exploration in the Gulf of Mexico?: 79<sup>th</sup> Annual International Meeting, SEG, Expanded Abstracts, 41–45, <https://doi.org/10.1190/1.3255750>.
- Mora, P., 1989, Inversion = migration + tomography: Geophysics, **54**, no. 12, 1575–1586, <https://doi.org/10.1190/1.1442625>.
- Pratt, R. G., 1999, Seismic waveform inversion in the frequency domain, part 1: Theory and verification in a physical scale model: Geophysics, **64**, no. 3, 888–901, <https://doi.org/10.1190/1.1444597>.
- Shen, X., I. Ahmed, A. Brenders, J. Dellinger, J. Etgen, and S. Michell, 2017, Salt model building at Atlantis with full-waveform inversion: 87<sup>th</sup> Annual International Meeting, SEG, Expanded Abstracts, 1507–1511, <https://doi.org/10.1190/segam2017-17738630.1>.
- Shen, X., I. Ahmed, A. Brenders, J. Dellinger, J. Etgen, and S. Michell, 2018a, Full-waveform inversion: The next leap forward in subsalt imaging: The Leading Edge, **37**, no. 1, 67b1–67b6, <https://doi.org/10.1190/tle37010067b1.1>.
- Shen, X., L. Jiang, J. Dellinger, A. Brenders, C. Kumar, M. James, J. Etgen, D. Meaux, R. Walters, and N. Abdullayev, 2018b, High resolution full waveform inversion for structural imaging in exploration: 87<sup>th</sup> Annual International Meeting, SEG, Expanded Abstracts, 1098–1102, <https://doi.org/10.1190/segam2018-2997202.1>.
- Sirgue, L., and R. G. Pratt, 2004, Efficient waveform inversion and imaging: A strategy for selecting temporal frequencies: Geophysics, **69**, no. 1, 231–248, <https://doi.org/10.1190/1.1649391>.
- Tang, Y., S. Lee, A. Baumstein, and D. Hinkley, 2013, Tomographically enhanced full wavefield inversion: 83<sup>rd</sup> Annual International

- Meeting, SEG, Expanded Abstracts, 1037–1041, <https://doi.org/10.1190/segam2013-1145.1>.
- Tarantola, A., 1984, Inversion of seismic reflection data in the acoustic approximation: *Geophysics*, **49**, no. 8, 1259–1266, <https://doi.org/10.1190/1.1441754>.
- Threadgold, I. M., K. Zembeck-England, P. G. Aas, P. M. Fontana, D. Hite, and W. E. Boone, 2006, Implementing a wide azimuth towed streamer field trial: The what, why and mostly how of WATS in Southern Green Canyon: 76<sup>th</sup> Annual International Meeting, SEG, Expanded Abstracts, 2901–2904, <https://doi.org/10.1190/1.2370129>.
- Wang, P., Z. Zhang, Z. Wei, and R. Huang, 2018, A demigration-based reflection full-waveform inversion workflow: 88<sup>th</sup> Annual International Meeting, SEG, Expanded Abstracts, 1138–1142, <https://doi.org/10.1190/segam2018-2997404.1>.
- Xu, S., D. Wang, F. Chen, Y. Zhang, and G. Lambaré, 2012, Full waveform inversion for reflected seismic data: 74<sup>th</sup> Conference and Exhibition, EAGE, Extended Abstracts, <https://doi.org/10.3997/2214-4609.20148725>.
- Yang, Z., S. Huang, and R. Yan, 2015, Improved subsalt tomography using RTM surface offset gathers: 85<sup>th</sup> Annual International Meeting, SEG, Expanded Abstracts, 5254–5258, <https://doi.org/10.1190/segam2015-5848366.1>.
- Zhang, Z., J. Mei, F. Lin, R. Huang, and P. Wang, 2018, Correcting for salt misinterpretation with full-waveform inversion: 88<sup>th</sup> Annual International Meeting, SEG, Expanded Abstracts, 1143–1147, <https://doi.org/10.1190/segam2018-2997711.1>.